Modified Hysteretic Current Control (MHCC) for Improving Transient Response of Boost Converter

Jen-Chieh Tsai, Chi-Lin Chen, Yu-Huei Lee, *Student Member, IEEE*, Hong-Yuan Yang, Ming-Shen Hsu, and Ke-Horng Chen, *Senior Member, IEEE*

***Abstract*—This paper proposes a modulated hysteretic current control (MHCC) technique to improve the transient response of a DC-DC boost converter, which suffers from low bandwidth due to the existence of the right-half-plane (RHP) zero. The MHCC technique can automatically adjust the on-time value to rapidly increase the inductor current, as well as to shorten the transient response time. In addition, based on the characteristic of the RHP zero, the compensation poles and zero are deliberately adjusted to achieve fast transient response in case of load transient condition and adequate phase margin in steady state. Experimental results show the improvement of transient recovery time over 7.2 times in the load transient response compared with the conventional boost converter design when the load current changes from light to heavy or vice versa. The power consumption overhead is merely 1%.**

***Index Terms*—Boost converter, hysteretic current control (HCC), load transient response, right-half-plane (RHP) zero.**

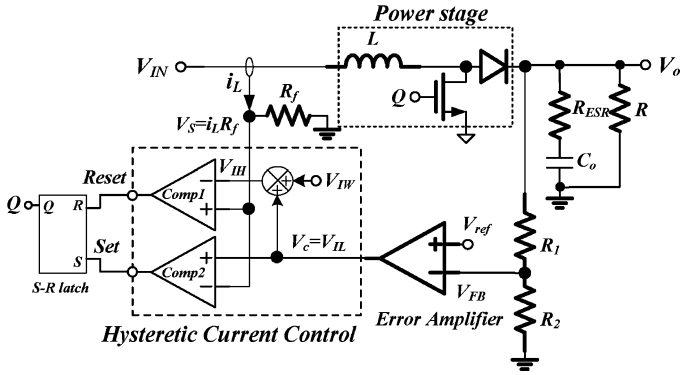

Fig. 1. Proposed HCC technique uses an error amplifier to enhance the regulation accuracy.

I. Introduction

LIGHT emission diode (LED) backlights have become increasingly popular in the recent green power mainstream. LED backlights have better color gamut and consumes less power than the cold cathode fluorescent lamp (CCFL) backlights [1], [2]. In addition, start-up time is shorter than that of the latter. As a result, recent liquid crystal display (LCD) backlight systems have gradually shifted to LED backlight to enhance display quality and power consumption.

One of the main characteristics that may affect image quality is backlight uniformity. Therefore, a boost converter is widely utilized for LED backlight display systems to step up low-input voltage to high-output voltage for driving a number of LEDs in series. The brightness of the LED can be easily adjusted by the digital dimming control method and by the constant current sink circuit [3]–[5], thereby achieving precise backlighting control. Additionally, the voltage across the current sink circuit must be minimized to reduce power consumption. As a result, using a minimum output voltage of the boost converter to activate the LED strings can enhance the efficiency of the LED driver. To provide good driving capability for controlling the brightness of LED, the boost converter is required to handle massive instant load variation to maintain the image quality. Therefore, the transient response is also an essential design issue because the large output voltage drop on the boost converter may result in the insufficient driving voltage for activating the LEDs.

Due to its low power consumption, the hysteretic current control (HCC) technique is selected as the modulation method for the LED backlight [6]. However, the voltage regulation performance of the HCC technique is inferior to that of the pulsewidth modulation (PWM) method [7] because the inductor current level varies under the different load conditions. Thus, in the proposed HCC technique, an error amplifier is utilized to form a voltage loop to improve regulation accuracy, as illustrated in Fig. 1. In addition, a pre-defined current hysteresis window, $V_{\rm IW}$, can limit the inductor current within it to guarantee a restricted output voltage ripple, as expressed in (1) [8]. $V_{\rm ESR}$ is the voltage across the equivalent series resistance (ESR) and $V_{\rm Co}$ is the voltage across the capacitor Co. The regulation performance and power consumption can therefore be ensured by the proposed HCC technique

$$\Delta v_o = V_{\rm ESR} + V_{C_o} \tag{1}$$

Furthermore, the proposed HCC technique has fast transient response because the trailing and leading edges can rapidly react to the output load variation. The on-time of the pulsewidth signal adaptively increases or decreases when the load current suddenly increases or decreases, respectively. Similarly, the off-time can be modulated to improve the transient response time due to the HCC window controlled by the error amplifier.

Unfortunately, unlike the design of buck converters, the transient response of the boost converter is limited by the existence of the RHP zero in continuous conduction mode (CCM) because the RHP zero remains in both of the PWM control (in either voltage- or current-mode) and the HCC technique [9], [10]. In

Manuscript received July 15, 2010; revised October 04, 2010; accepted November 26, 2010. Date of publication February 14, 2011; date of current version July 27, 2011. This paper was recommended by Associate Editor E. Alarcon.

The authors are with the Institute of Electrical Control Engineering, National Chiao Tung University, Hsinchu 300, Taiwan (e-mail: khchen@cn.nctu.edu.tw).

Color versions of one or more of the figures in this paper are available online at http://ieeexplore.ieee.org.

Digital Object Identifier 10.1109/TCSI.2011.2106231

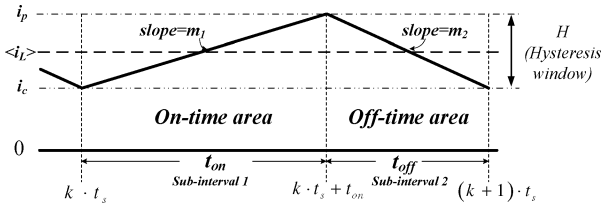

Fig. 2. Inductor current waveform is limited with the hysteresis window defined by the HCC technique.

a conventional boost converter design, the discontinuous conduction mode (DCM) is widely used to obtain simple system compensation due to the existence of the RHP zero at high frequencies. However, the load transient response in DCM hardly meets the requirement of the LED backlight. As a result, eliminating the effect of the RHP zero is a proper solution in a boost converter to speed up the load transient response. The MHCC technique is proposed to improve the transient response in the DC-DC boost converters in order to automatically adjust the on-time value and rapidly increase the inductor current, thereby shortening the transient response time. Moreover, it can deliberately adjust the compensation poles and zero to achieve fast transient response in case of load transient condition and yield adequate phase margin (PM) in steady state.

The paper is organized according to the following sections. Section II shows the small-signal analysis of the HCC technique indicating the system compensation for ensuring stability. Section III describes the operation of the proposed MHCC technique to achieve the fast transient response. A comparison is also shown to demonstrate the performance. Circuit implementations are illustrated in Section IV. Experimental results are discussed in Section V to prove the performance and precision of the proposed MHCC technique. Finally, a conclusion is made in Section VI.

II. Small-Signal Analysis and System Compensation With HCC Technique

A. Small-Signal Modeling of the HCC Technique

As depicted in Fig. 2, the HCC technique senses the inductor current and limits it within a hysteresis window, defining the upper and lower current bands. The inductor current rises to reach the upper band of the hysteresis window when the N-MOSFET turns on during $t_{\rm on}$ period [11]. In contrast, the inductor current falls to reach the lower band of the hysteresis window when the N-MOSFET turns off during the $t_{\rm off}$ period. This simple HCC technique exhibits fast dynamic characteristics.

The switching period t_s, as expressed in (2), is equal to the sum of the on-time $t_{\rm on}$ and the off-time $t_{\rm off}$ in the CCM operation. The value of $t_{\rm off}$ can be written as (3) according to the waveform in Sub-interval 2

$$t_s = t_{\rm on} + t_{\rm off} \tag{2}$$

$$t_{\rm off} = \frac{L \cdot H}{(v_o - v_{\rm in})}. \tag{3}$$

The peak inductor current, i_p, can be expressed as (4) by $t_{\rm on}$ and the average inductor current $\langle i_L \rangle$.

$$i_p = \langle i_L \rangle + \frac{v_{\rm in}}{2L} t_{\rm on} \tag{4}$$

Given the small-signal analysis, the value of each variable can be written as the summation of the DC term, whose perturbation as shown in (5). The duty cycle, d, and its complementary value, d', also are defined in (6)

$$t_s = T_s + \hat{t}_s, \quad t_{\rm on} = T_{\rm on} + \hat{t}_{\rm on}, \quad \text{and}$$
$$t_{\rm off} = T_{\rm off} + \hat{t}_{\rm off} = d' t_s \tag{5}$$
$$d = D + \hat{d} \quad \text{and} \quad d' = 1 - d = D' - \hat{d}. \tag{6}$$

Hence, (2) and (3) can be rewritten as (7) and (8), respectively

$$\left(T_s + \hat{t}_s\right) = (T_{\rm on} + \hat{t}_{\rm on}) + (T_{\rm off} + \hat{t}_{\rm off}) \tag{7}$$

$$T_{\rm off} + \hat{t}_{\rm off} = \frac{LH}{(V_o + \hat{v}_o - V_{\rm in} - \hat{v}_{\rm in})}. \tag{8}$$

Keeping the first-order AC terms, the small-signal equation can be derived in (9)

$$\hat{t}_s = \hat{t}_{\rm on} + \hat{t}_{\rm off}, \quad \hat{d} = \frac{\hat{t}_{\rm on} - D\hat{t}_s}{T_s}$$
$$\hat{t}_{\rm off} = -\frac{LH}{(V_o - V_{\rm in})^2}(\hat{v}_o - \hat{v}_{\rm in}). \tag{9}$$

Similarly, $\hat{i}_p$ and $\hat{t}_{\rm on}$, are expressed in (10) as

$$\hat{i}_p = \hat{i}_L + \frac{(V_{\rm in}\hat{t}_{\rm on} + T_{\rm on}\hat{v}_{\rm in})}{2L} \quad \text{and}$$
$$\hat{t}_{\rm on} = \frac{2L}{V_{\rm in}}(\hat{i}_p - \hat{i}_L) - \frac{T_{\rm on}}{V_{\rm in}}\hat{v}_{\rm in}. \tag{10}$$

Therefore, the small-signal duty cycle is derived as (11)

$$\hat{d} = \left(D' \left(\frac{2L}{V_{\rm in}}(\hat{i}_p - \hat{i}_L) - \frac{T_{\rm on}}{V_{\rm in}}\hat{v}_{\rm in} \right) + \frac{LHD}{(V_o - V_{\rm in})^2}(\hat{v}_o - \hat{v}_{\rm in}) \right) \cdot (T_s)^{-1}. \tag{11}$$

Given that $DT_S = H/(V_{\rm in}/L)$ and $1/(V_o - V_{\rm in}) = 1/(DV_o)$, (12) can be derived from (11)

$$\hat{d} = \left(\frac{2D'D}{H}(\hat{i}_p - \hat{i}_L) \right) + \frac{D'}{V_o}(\hat{v}_o) - \left[\left(\frac{T_{\rm on}}{V_{\rm in}} \cdot D' + \frac{LHD}{(V_o - V_{\rm in})^2} \right) (\hat{v}_{\rm in}) \right] \cdot (T_s)^{-1}. \tag{12}$$

Due to the equation shown in (13), $\hat{d}$ is shown in (14)

$$\left(\frac{LHD}{(V_o - V_{\rm in})^2} \right) \cdot (T_s)^{-1} = \frac{D'}{V_o} \tag{13}$$

$$\hat{d} = \frac{2DD'}{H}(\hat{i}_P - \hat{i}_L) - \frac{1}{V_o}\hat{v}_{\rm in} + \frac{D'}{V_o}\hat{v}_o. \tag{14}$$

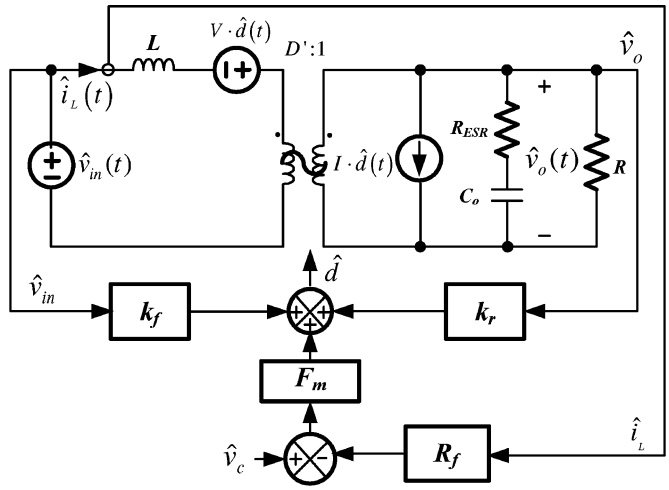

Fig. 3. Small-signal model of the boost converter under the hysteretic current mode control.

Because of the DC equivalent equations above, (15) and (16) can be derived as follows:

$$\hat{d} = F_m(\hat{v}_C - R_f\hat{i}_L) + k_f \cdot \hat{v}_{\text{in}} + k_r \cdot \hat{v}_o \tag{15}$$

$$\hat{v}_C = \hat{i}_p R_f, \quad F_m = \frac{2DD'}{HR_f},$$

$$k_f = -\frac{1}{V_o}, \quad \text{and} \quad k_r = \frac{D'}{V_o}. \tag{16}$$

The HCC technique can determine the inductor peak current by the intersection of the error signal and the current-sensing signal. The small-signal model [12]–[14] of the boost converter with a hysteretic current mode control is illustrated in Fig. 3. The control-to-output transfer function is shown in (17), where R is the output load impedance, R_f is the current sensing gain, and R_{ESR} is the equivalent series resistance of the output capacitor, C_o

$$G_{vc} = \frac{\hat{v}_o}{\hat{v}_c} = \frac{F_m \cdot G_{vd}}{1 - k_r \cdot G_{vd} + F_m \cdot G_{id} \cdot R_f} \tag{17}$$

where

$$G_{vd} = \left.\frac{\hat{v}_o}{\hat{d}}\right|_{\hat{v}_{\text{in}}=0} = \frac{V_o}{D'} \cdot \frac{\left(1 - s\frac{L}{D'^2R}\right)(1 + sR_{\text{ESR}}C_o)}{1 + s\frac{L}{RD'^2} + s^2\frac{LC_o}{D'^2}}$$

and

$$G_{id} = \left.\frac{\hat{i}_L}{\hat{d}}\right|_{\hat{v}_{\text{in}}=0} = \frac{2 \cdot V_o}{D'^2R} \cdot \frac{\left(1 + s\frac{RC_o}{2}\right)}{1 + s\frac{L}{RD'^2} + s^2\frac{LC_o}{D'^2}}. \tag{18}$$

Formula (17) can be simplified as (19) because $F_m\ G_{id}\ R_f \gg 1 - k_r\ G_{vd}$ in the proposed design, according to the design values

$$G_{vc} = \frac{\hat{v}_o}{\hat{v}_c} = \frac{F_m \cdot G_{vd}}{F_m \cdot G_{id} \cdot R_f} = \frac{1}{R_f}\frac{G_{vd}}{G_{id}}$$

$$= G_{vc0}\frac{\left(1 - \frac{s}{\omega_{z(\text{RHP})}}\right)\left(1 + \frac{s}{\omega_{z(\text{ESR})}}\right)}{\left(1 + \frac{s}{\omega_{p1}}\right)} \tag{19}$$

where

$$G_{vc0} = \frac{D'R}{2R_f}, \quad \omega_{p1} = \frac{2}{RC_o}$$

and

$$\omega_{z(\text{RHP})} = \frac{D'^2R}{L}, \quad \omega_{z(\text{ESR})} = \frac{1}{R_{\text{ESR}}C_o} \tag{20}$$

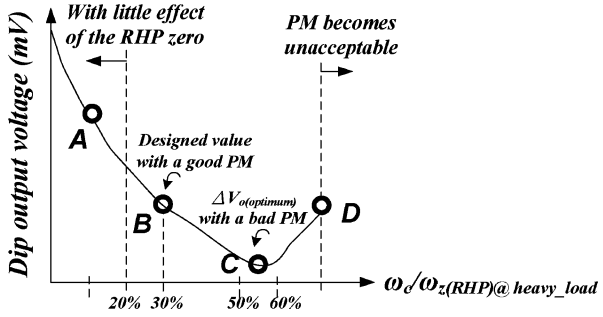

Fig. 4. Dip output voltage versus the ratio of the ω_c and $\omega_{z(\text{RHP})}$ for showing the effect of the RHP zero.

The system contains one dominant pole, ω_{p1}, and two zeros, which include one RHP zero, $\omega_{z(\text{RHP})}$, and one LHP zero, $\omega_{z(\text{ESR})}$. The frequency response of the HCC technique is similar to that of the current-mode PWM technique. Thus, the proportional-integral (PI) compensation [15] is suitable to achieve system compensation in the proposed structure. The transfer function of the PI compensator is shown in (21). Compensation zero ω_{zc1} is used to cancel the effect of the system pole ω_{p1}. Then, ω_{pc1} forms the dominant pole to stabilize the system, and ω_{pc2} can help decrease the high-frequency gain to eliminate the effect of $\omega_{z(\text{RHP})}$

$$G_c = G_{c0}\frac{\left(1 + \frac{s}{\omega_{zc1}}\right)}{\left(1 + \frac{s}{\omega_{pc1}}\right)\left(1 + \frac{s}{\omega_{pc2}}\right)}. \tag{21}$$

The existence of the RHP zero influences the system bandwidth. As illustrated in (20), the effect of RHP zero becomes worse at heavy loads. The crossover frequency, ω_c, is generally designed to be smaller than 10%–20% of the $\omega_{z(\text{RHP})}$ when it is under a heavy load, as shown in Fig. 4. The output voltage, V_o, has no dip voltage in case of load current variation because $\omega_{z(\text{RHP})}$ is remote from the crossover frequency. In other words, the RHP zero has minimal effect on the dip output voltage. However, the transient response is too slow, resulting in a large undershoots voltage due to the small system bandwidth. Increasing the crossover frequency can shorten the transient response and obtain a small undershoot voltage; however, a large dip voltage is also derived because of the existence of the RHP zero. As a result, there exists an optimum ratio between ω_c and $\omega_{z(\text{RHP})}$ for obtaining the smallest dip output voltage, which is labeled as $\Delta V_{o(\text{optimum})}$ at Point C, as well as the shortest transient response period. Nevertheless, the PM at this optimum dip voltage is not desirable because of the existence of the $\omega_{z(\text{ESR})}$ and ω_{pc2} generated from the PI compensator. Therefore, the system bandwidth needs to be extended to ensure a stable transient response that removes the restriction of 10%–20% RHP zero. The designed value of this work is set at Point B, which is approximately 30% of the RHP zero aiming for a better PM.

B. Closed-Loop Analysis With the PI Compensation

A closed-loop diagram of the boost converter with the HCC technique is shown in Fig. 5. The loop gain $T(s)$ is illustrated in (22). Here, $H(s)$ is the sensor gain, which is equal to $R_2/(R_1 + R_2)$, whereas $G_c(s)$ is composed of an error amplifier and a PI

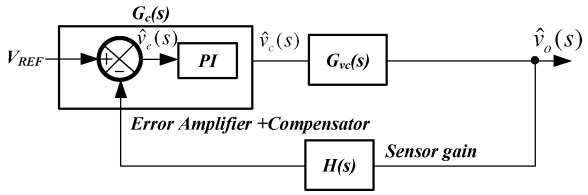

Fig. 5. Simplified feedback system of the HCC regulator.

compensator that represents the transfer function of the compensation network. The PI compensator contributes the compensation poles and zero, as described in (21)

$$T(s) = G_{vc}(s) \cdot H(s) \cdot G_c(s). \tag{22}$$

Due to the decrease of the frequency of RHP zero $\omega_{z(\mathrm{RHP})}$ at heavy loads, the compensation zero, ω_{zc1}, in the PI compensator is designed to cancel the effect of the system pole, ω_{p1}, to extend the system bandwidth. However, at heavy loads, the crossover frequency is limited by $\omega_{z(\mathrm{RHP})}$, resulting in an improper system compensation, as depicted in Fig. 6(a). According to Fig. 4, the ratio of ω_c and $\omega_{z(\mathrm{RHP})}$ has an optimum value when the dip output voltage is the major concern.

In contrast, the bandwidth worsens due to the decrease in ω_{p1} at light loads. As illustrated in Fig. 6(b), the compensation zero can be adaptively adjusted within a stable region. The maximum value of ω_{zc1} is determined by the PM because there are two poles at low frequencies once the compensation zero moves toward high frequencies. In addition, the minimum value of ω_{zc1} is determined by the minimum value between $\omega_{z(\mathrm{RHP})}$ and ω_{pc2} because a decrease in ω_{zc1} also causes a decrease in ω_{pc2} when using the PI compensator. However, the minimum value of ω_{zc1} is no longer decided by $\omega_{z(\mathrm{RHP})}$ because ω_{pc2} is smaller than $\omega_{z(\mathrm{RHP})}$ at light loads. To obtain a better PM at light loads, ω_{zc1} must be adaptively moved to effectively cancel the effect of the system pole ω_{p1} under the different output load conditions.

An adaptive compensation zero can ensure a good PM; however, improving the transient response is difficult because of the limitation in the low-frequency RHP zero. Therefore, the MHCC technique includes an adaptive compensation control (ACC) to obtain a fast transient response and a good PM in steady state.

III. Proposed MHCC Technique for Fast Transient Response

The proposed MHCC architecture, as shown in Fig. 7, can ensure a limited output ripple and adjust the trailing and leading edges for fast transient response. Moreover, the ACC technique can rapidly regulate the output of the error amplifier to speed up the transient response and guarantee good PM in the steady state. The difference in the voltages between the upper band V_{IH} and the lower band V_{IL} forms the hysteresis current window, which is the product of I_{hys} and R_{hys}. Here, V_{IL} is equal to the output voltage V_{eao} of the error amplifier for improving the accuracy of load regulation. The ACC technique is composed of the adaptive resistance and capacitance, which are controlled by the ACC controller. As a result, the compensation poles and zero can be adaptively adjusted in the load transient and steady state.

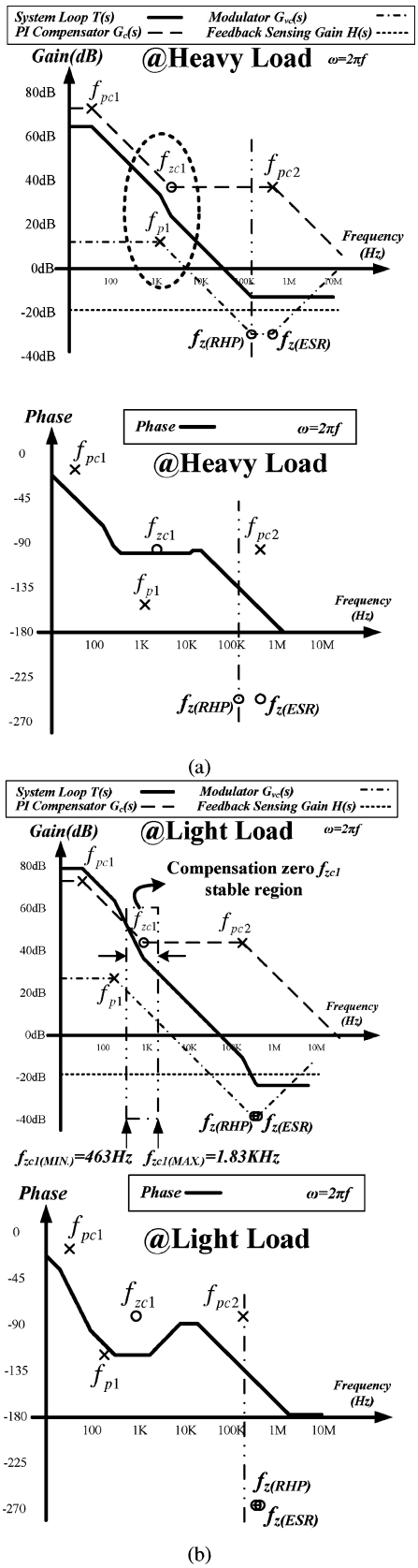

Fig. 6. Compensated loop gain $T(s)$ (a) at heavy loads and (b) at light loads.

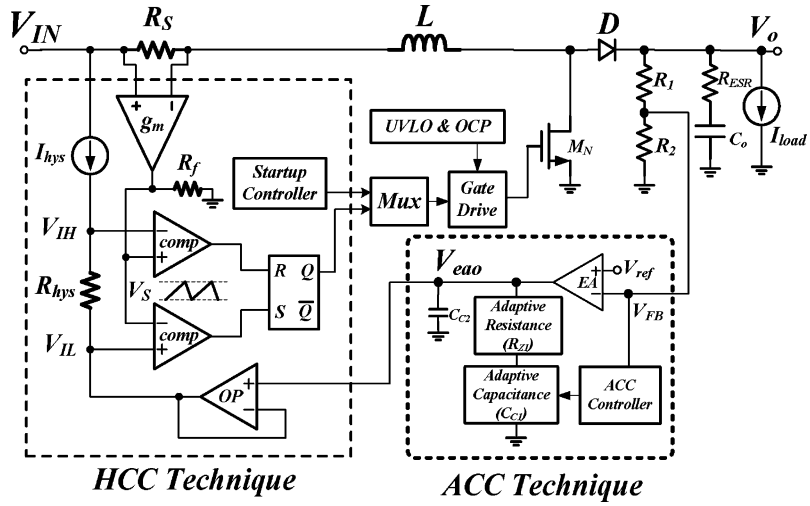

Fig. 7. System architecture of the proposed boost converter with the proposed MHCC technique.

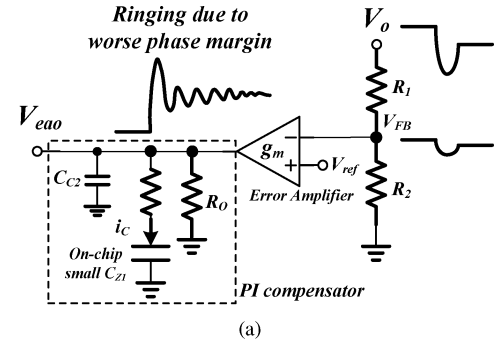

(a)

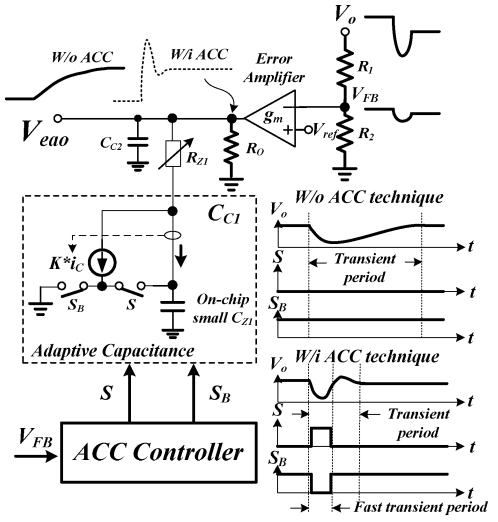

(b)

Fig. 8. PI compensator (a) with a small on-chip capacitor, (b) with and without the ACC technique.

A. Adaptive Compensation Control (ACC) Technique

As presented in Fig. 8(a), the PI compensator is connected at the output $V_{\rm eao}$ of the error amplifier. Given that only a small on-chip capacitor is allowed in the IC fabrication, the small feedback voltage $V_{\rm FB}$ may cause a large voltage variation at $V_{\rm eao}$ when the compensation zero ω_{zc1} is located at high frequencies, resulting in insufficient PM.

A pseudo large compensation capacitance is derived through the adaptive capacitance C_{C1}, as shown in Fig. 8(b). The large capacitance can be generated through a mirrored AC current, $K * i_c$, connected to the ground [16] that only allows a small current to flow into the small on-chip capacitor C_{Z1}. Thus, the on-chip compensation can be achieved by the implementation of the small capacitor C_{Z1}. In addition, when the load transient response occurs, V_o would drop as well as $V_{\rm FB}$, triggering fast transient operation [17] with the ACC control. Here, S is the control signal, indicating the period of the fast transient response, for the auxiliary switches to return the large compensation capacitance to the small on-chip capacitor C_{Z1} in the transient period. Consequently, the response at $V_{\rm eao}$ is accelerated for rapid reaction to the output load variations in the boost converter.

Moreover, $V_{\rm eao}$ can have a stable settling behavior due to the large transient current, which can be redirected to the ground. Similar to the off-chip compensation zero, a pseudo low-frequency compensation zero is used to cancel the effect of the output system pole. As mentioned above, the bandwidth is small because of the RHP zero. Furthermore, the ACC technique can deliberately control the switches S and S_B to improve the transient response. This modifies the pseudo compensation poles and zero to obtain a small dip output voltage and fast transient response time, as shown in Fig. 8(b). Thus, the PI compensator can generate two poles, ω_{pc1} and ω_{pc2}, and one zero, ω_{zc1}, as shown in (23), to compensate the proposed structure.

$$\omega_{pc1} \approx \frac{1}{R_o C_{C1}}, \quad \omega_{pc2} \approx \frac{1}{R_{Z1} C_{C2}}, \quad \omega_{zc1} \approx \frac{1}{R_{Z1} C_{C1}}. \tag{23}$$

According to Fig. 4, the ratio of ω_c to $\omega_{z(\rm RHP)}$ can be increased for a short period by the ACC technique to obtain a higher bandwidth. Thus, the dip output voltage would not be significantly increased when the operation points from B toward a higher ratio of ω_c to $\omega_{z(\rm RHP)}$. That is, the fast transient period will push the operation point from Point B to Point C, and then to Point D. After the fast transient period, it is pushed back

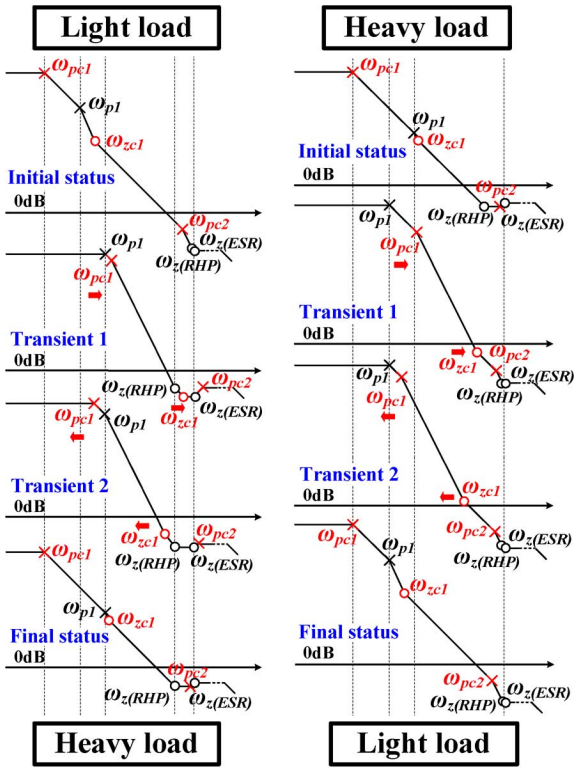

Fig. 9. The compensation poles and zeros controlled by the ACC technique (a) when load current changes from light to heavy and (b) when load current changes from heavy to light.

to Point B to ensure a better PM value. The fast transient period only occupies one fraction of the transient period. The dip output voltage can be smaller compared to that without the ACC technique. The value of $V_{\rm eao}$ can be rapidly settled to its stable level; thus the MHCC technique can achieve a fast transient response and a small dip output voltage without being limited by the RHP zero.

The operation of the ACC technique needs careful control of the compensation poles and zeros during the fast transient period. Basically, the fast transient period contains two stages, as indicated by the signal S in Fig. 8(b): Transient 1 and 2. At the Transient 1 stage, the mirrored AC current is fully redirected to the small on-chip capacitor to recover rapidly the voltage level of $V_{\rm eao}$. Then, the Transient 2 stage needs to detect the valley point of the dip output voltage to pull back the compensation poles and zeros to the position that ensures that the system has a better PM value. Moreover, to achieve the exact system pole-zero cancellation, the compensation resistance R_{Z1} is adjusted according to the different load conditions. This ensures the adequate system PM under different output load conditions.

The locations of the compensation poles and zeros controlled by the ACC technique are shown in Fig. 9. When the load changes from light to heavy [Fig. 9(a)], the ACC technique activates the fast transient procedure. In the Transient 1 period, the system bandwidth can be largely extended by moving ω_{pc1}, ω_{pc2}, and ω_{zc1} to the high frequencies. This is because the adaptive capacitance circuit returns the compensation capacitance to a small value, thereby triggering the fast loop response of the proposed structure. Additionally, the period of Transient 2 can pull back the compensation poles and zero to ensure system stability. In the final status, the adaptive capacitance is set to a steady-state value as the initial status. The adaptive resistance circuit can also move the compensation zero ω_{zc1} to cancel the effect of ω_{p1} for yielding the adequate PM. A similar operation is activated when the load changes from heavy to light as depicted [Fig. 9(b)].

B. Compensation of the Modulation Techniques

The switching frequency of the PWM mode is fixed, and the switch has to turn on and off every switching cycle. The recovery time takes a longer time, as shown in Fig. 10(a), when the output current changes from light to heavy. In contrast, the inductor current in the HCC technique is controlled within two boundaries: i_c, which is determined by the error amplifier, and $i_c+\Delta I$, as depicted in Fig. 10(b) where ΔI is the current hysteresis window [18]–[20]. The recovery time can be shortened because the on-time value is not limited by the maximum on-time value in the HCC control technique. The switching period can be extended; thus, the inductor current can be rapidly increased to the regulated level. The current of $i_{l\_{\rm sub1}}$ obtains additional time to reach the boundary, $i_c + \Delta I$. The switching frequency of the boost converter slows when the load current changes from light to heavy. Therefore, the inductor charging period is extended to raise rapidly the inductor current level, shortening the transient response period and minimizing the transient dip voltage. This is the reason the recovery time of the HCC technique is faster than that of the current-mode PWM technique.

The proposed MHCC technique rapidly regulates the output of the error amplifier to shorten the transient response time. However, the system bandwidth is limited by the RHP zero in the boost converter [21]–[23]. The MHCC technique utilizes the characteristics of the RHP zero to initiate a large control signal due to the inferior PM to recover rapidly the voltage level at the output of the error amplifier. However, the inferior PM cannot ensure a stable operation in the steady state. The MHCC technique can adaptively adjust the compensation poles and zeros to low frequencies to guarantee system stability. During the transient response, if i_c is able to rise and fall quickly, the recovery time is shortened, as shown in Fig. 10(c).

IV. Circuit Implementations

The proposed MHCC technique contains two main blocks: the HCC and the ACC circuits. The current sensor and the fixed hysteretic current window circuit constitute the HCC circuit. The adaptive compensation resistance, the capacitance circuits, and the ACC controller constitute the ACC circuit.

A. Current Sensor

The HCC technique needs to sense the full-range inductor current. Thus, an accurate current sensor is required. As depicted in Fig. 11, a small value-sensing resistor R_S is connected in series with the inductor to sense the full-range inductor current. A slight reduction in the power conversion efficiency may ensue in this simple procedure. The transistors M_1 and M_2 are biased by the same bias current I_1. Thus, $V_{SG1} = V_{SG2}$. According to the current values labeled in Fig. 11, (24) can be de-

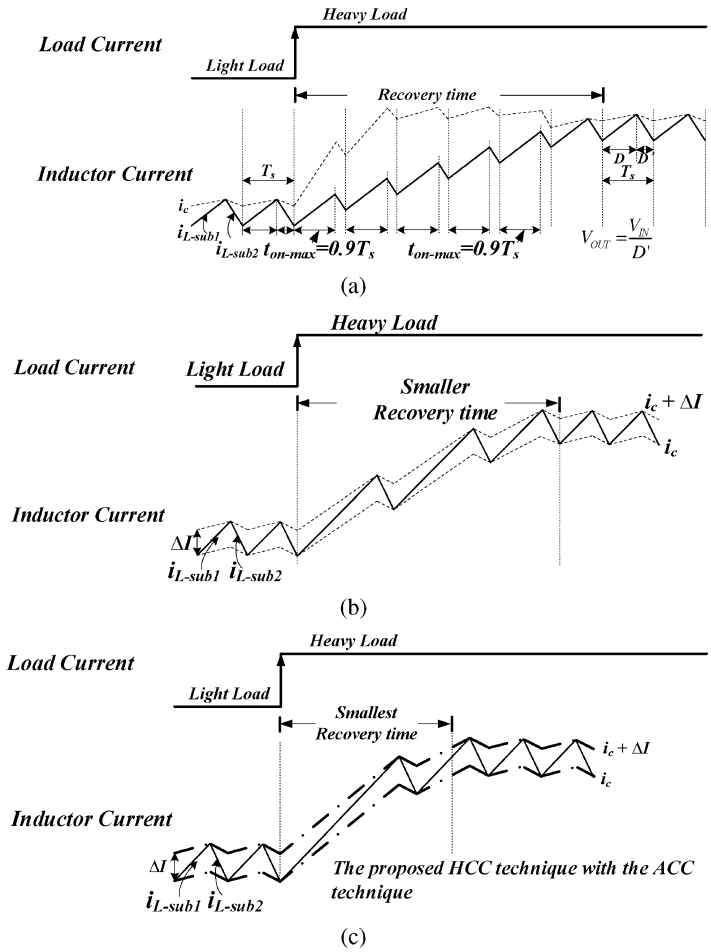

Fig. 10. Recovery time during light load to heavy load. (a) Waveforms controlled by the PWM technique. (b) Waveforms controlled only by the HCC technique. (c) Waveforms controlled by the proposed MHCC technique.

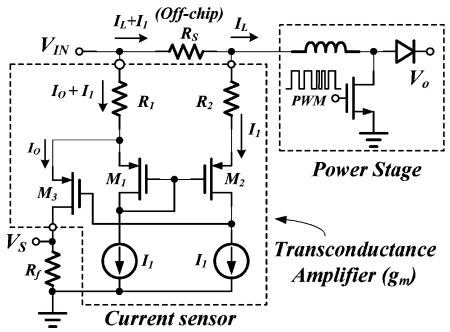

Fig. 11. Schematic of current sensor.

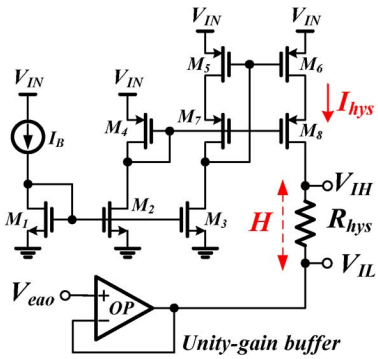

Fig. 12. Fixed hysteretic current window circuit.

rived and simplified as (25) if $R_1 = R_2$ under a good layout matching result

$$V_{SG1} + (I_o + I_1)R_1 = V_{SG2} + (I_L + I_1)R_S + I_1R_2 \tag{24}$$

$$I_o = I_L \cdot R_S/R_1. \tag{25}$$

The sensing signal V_S can be expressed in (26) and used to represent the full-range inductor current. Hence, the value of V_S can be scaled by the ratio of $(R_S * R_V)$ to R_1. According to the operation of the HCC technique, the value of V_S is limited within the hysteresis window, which is controlled by the fixed hysteretic window circuit

$$V_S = I_o R_f = I_L\,(R_S \cdot R_f/R_1) \propto I_L. \tag{26}$$

B. Fixed Hysteretic Current Window Circuit

The fixed hysteretic current window circuit is designed to control accurately the output ripple for ensuring the regulation performance, as shown in Fig. 12. The lower band of the fixed hysteretic current window is controlled by the output of the error

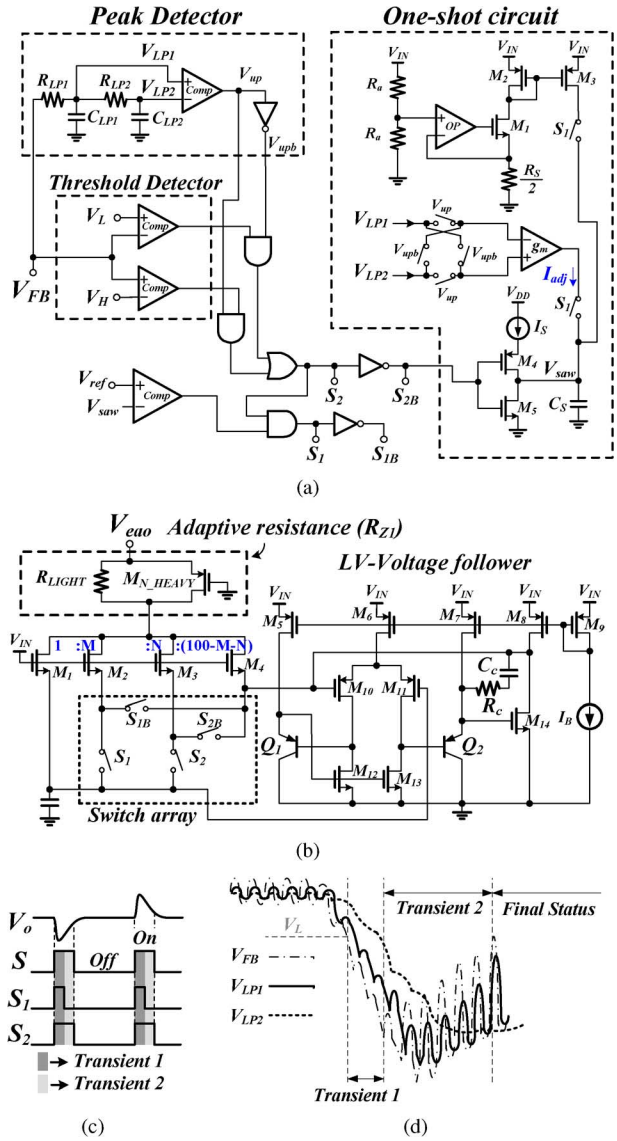

Fig. 13. (a) Schematic of the ACC controller. (b) Adaptive capacitance circuit. (c) Time diagram of the switch control signals. (d) Waveforms of the peak detector.

amplifier, $V_{\rm eao}$. Thus, a unity-gain buffer used to filter out the switching noise can generate the lower band V_{IL}. The hysteretic window is easily generated by adding an IR-drop to V_{IL}. The value of the IR-drop is derived by a constant current flowing through a hysteresis resistor $R_{\rm hys}$. As a result, the upper band V_{IH} can be expressed by (27). The cascaded current mirror M_6 and M_8 can suppress the channel length modulation effect to obtain higher accuracy

$$V_{IH} = V_{IL} + I_{\rm hys} \cdot R_{\rm hys}. \tag{27}$$

C. Adaptive Capacitance and Resistance Circuits and the ACC Controller

The fast transient mechanism is triggered by the threshold detector in Fig. 13(a). Once the feedback voltage $V_{\rm FB}$ is higher or lower than V_{IH} or V_{IL}, the ACC controller begins to control the fast transient procedure. The ACC technique can speed up the transient response by two transient procedures: Transient 1 and Transient 2 stages. The Transient 1 stage is simply decided by a one-shot circuit to increase rapidly the voltage of $V_{\rm eao}$. As depicted in Fig. 13(a), the one-shot period can be determined by (28)

$$\begin{aligned} T_{\rm one\text{-}shot} &= \frac{C_S \cdot V_{\rm ref}}{I_S + \frac{V_{\rm IN}}{R_S} + I_{\rm adj}} \\ &= \frac{C_S \cdot V_{\rm ref}}{I_S + \frac{V_{\rm IN}}{R_S} + g_m |V_{LP1} - V_{LP2}|}. \end{aligned} \tag{28}$$

The one-shot period is inversely proportional to the input voltage because the one-shot value should be shortened under a large input voltage. Moreover, bigger overshoot and undershoot output voltages need longer one-shot values. The adaptive resistance is shown in Fig. 13(b), which is equal to the value of two resistances in parallel (i.e., $R_{Z1} = R_{\rm LIGHT} || R_{MN\_{\rm HEAVY}}$). The maximum equivalent value of R_{Z1} is designed as $R_{\rm LIGHT}$ at light loads because the transistor $M_{N\_{\rm HEAVY}}$ operating in the cut-off region causes $R_{MN\_{\rm HEAVY}}$ to be sufficiently large to be ignored. The adaptive capacitance contains the voltage follower designed by the low-voltage operational amplifier to ensure the accurate current mirror constituted by the transistors M_1–M_4. The input common-mode range can be set from 0.4 to 1.9 V. The time diagram of the switch control signals is shown in Fig. 13(c). The control signal S, shown in Fig. 8(b), represents the fast transient period including Transients 1 and 2. During Transient 1, the switches in the switch array of Fig. 13(b) are all enabled by the detail control signals of S_1 and S_2 from the ACC controller. During Transient 2, the S_2 is still on to derive the correct operation of the ACC technique.

Consequently, the current mirror array in Fig. 13(b) can determine the value of the pseudo capacitance $C_{\rm pseudo}$. The ratio of the current mirror array is 1:M:N:(100-M-N). In this paper, $M = 65$ and $N = 30$. Thus, $C_{\rm pseudo}$ changes from $(1+K)\,C_{Z1}$ to the value, as shown in (29). Here, K is the enlarged factor

$$\begin{aligned} C_{\rm pseudo} &= \left(1 + \frac{100 - M - N}{1 + M + N}\right) C_{Z1} \\ &= \left(1 + \frac{100 - 65 - 30}{1 + 65 + 30}\right) \times 2pF \approx 2.1pF. \end{aligned} \tag{29}$$

In other words, 95% of the mirrored current is directed to the small capacitor C_{Z1} to rapidly increase the voltage level of $V_{\rm eao}$. As a result, the system bandwidth can be extended, and the drop voltage can be reduced. However, the PM is not sufficient to ensure a stable operation. Thus, the one-shot timing control in (28) depends on $V_{\rm IN}$ and V_o to avoid oscillation.

After the Transient 1 stage, the Transient 2 stage is determined by the valley of the output voltage. Thus, a peak detector in Fig. 13(a) is required to decide the period of the Transient 2 stage. As illustrated in Fig. 13(d), the feedback signal $V_{\rm FB}$ can be filtered by two low-pass filters, $(R_{\rm LP1}, C_{\rm LP1})$ and $(R_{\rm LP2}, C_{\rm LP2})$, to generate two output signals, $V_{\rm LP1}$ and $V_{\rm LP2}$. In the Transient 2 stage, the switches in Fig. 13(b) are conservatively set to increase $C_{\rm pseudo}$ to the value, as shown in (30)

$$\begin{aligned} C_{\rm pseudo} &= \left(1 + \frac{100 - N}{1 + N}\right) C_{Z1} \\ &= \left(1 + \frac{100 - 30}{1 + 30}\right) \cdot 2pF \approx 6.5pF. \end{aligned} \tag{30}$$

TABLE I
LOCATION LIST OF ALL POLES AND ZEROS IN MHCC STRUCTURE WITH TRANSIENT FROM LIGHT LOAD TO HEAVY LOAD

Status	Dominant-pole (f_{pc1})	System-pole (f_{p1})	Zero (f_{zc1})	High freq. pole (f_{pc2})	RHP zero ($f_{z(RHP)}$)	ESR zero ($f_{z(ESR)}$)	DC Gain (dB)	UGF	Phase (deg)
⓪Light Load (70mA)	25	273	916	191K	446K	468K	78.6	63K	71
Output load current changes from light load (70mA) to heavy load (270mA)									
①Transient 1	1.7K	1.1K	225K	700K	116K	468K	66.9	70K	-9
②Transient 2	701	1.1K	73K	550K	116K	468K	66.9	45K	13
③Heavy Load (270mA)	26	1.1K	1.8K	377K	116K	468K	66.9	34K	71

TABLE II
LOCATION LIST OF ALL POLES AND ZEROS IN MHCC STRUCTURE WITH TRANSIENT FROM HEAVY LOAD TO LIGHT LOAD

Status	Dominant-pole (f_{pc1})	System-pole (f_{p1})	Zero (f_{zc1})	High freq. pole (f_{pc2})	RHP zero ($f_{z(RHP)}$)	ESR zero ($f_{z(ESR)}$)	DC Gain (dB)	UGF	Phase (deg)
⓪ Heavy Load (270mA)	26	1.1K	1.8K	377K	116K	468K	66.9	34K	71
Output load current changes from heavy load (270mA) to light (70mA) load									
①Transient 1	1.7K	273	88K	277K	446K	468K	78.6	70K	25
②Transient 2	692	273	28K	218K	446K	468K	78.6	61K	50
③Light Load (70mA)	25	273	916	191K	446K	468K	78.6	63K	71

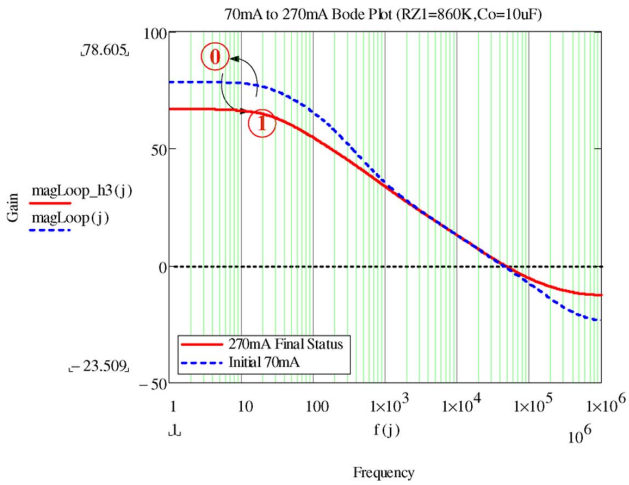

Fig. 14. Bode plot of the proposed boost converter with the HCC technique only.

During the Transient 2 stage, the compensation poles and zeros are pulled toward the origin to obtain a higher PM value. Once V_{LP1} is higher than V_{LP2}, the Transient 2 stage ends. After the detection of the peak value, the compensation poles and zeros are set to the positions that can guarantee an adequate PM value. Thus, C_{pseudo} is again equal to $(1+K)\,C_{Z1}$.

The Bode plot of the proposed boost converter with the HCC technique only is shown in Fig. 14. The loop gain varies with the different load conditions in the range of 65 to 80 dB. The crossover frequency is fixed at 50 kHz. The Bode plot of the proposed MHCC technique is shown in Fig. 15. The ACC technique activates the fast transient response when load current changes from light to heavy, as illustrated in Fig. 15(a). The loop crossover frequency is extended to 80 kHz during the fast transient period. The positions of all poles and zeros are listed in Table I. The value of f_c is set to approximately 30% of the

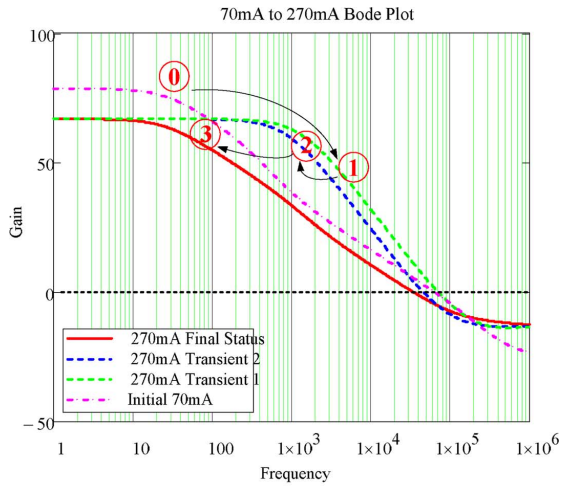

(a)

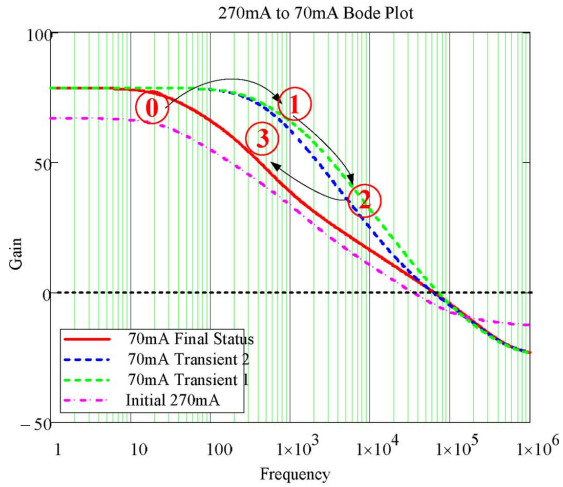

(b)

Fig. 15. Bode plot when load current changes (a) from light to heavy and (b) from heavy to light.

TABLE III
DESIGN SPECIFICATION OF THE PROPOSED MHCC STRUCTURE

Characteristics	Typical value	Unit
Supply Voltage (V_{in})	3.5~4.5	V
Output Voltage (V_o)	12	V
Output Current (I_{load})	70~270	mA
Input Inductor (L)	6.8	μH
Equilibrium series Resistance of the inductor (DCR)	45	mΩ
Output capacitor (C_O)	10	μF
Equilibrium series resistance of the output capacitor (R_{ESR})	50	mΩ
Operation temperature	0~100	℃

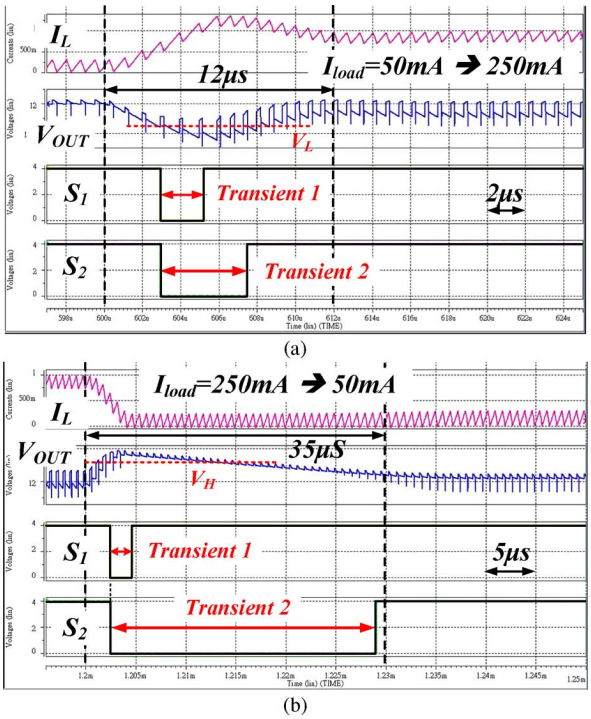

Fig. 16. Simulated results of the load transient response with the ACC technique (a) when load current changes from 50 to 250 mA and (b) when load current changes from 250 to 50 mA.

value of $f_{z(\mathrm{RHP})}$ at heavy loads, as presented in Fig. 4. Similarly, the Bode plot when the load current changes from heavy to light is shown in Fig. 15(b). The loop crossover frequency is also extended to 80 kHz during the fast transient period. Table II lists the relationship of the poles and zeros. At light loads, the value of f_c is set to approximately 30% of the value of f_{pc2}. The adaptive resistance moves both f_{zc1} and f_{pc2} toward the origin. Thus, f_{pc2} is smaller than $f_{z(\mathrm{RHP})}$ at light loads. In other words, f_{pc2} determines the position of f_c.

Simulation results of the load transient response in the proposed boost converter with the MHCC technique are shown in Fig. 16. When the load changes from 50 to 250 mA, as shown in Fig. 15(a), the ACC technique can ensure the system stability, voltage regulation in steady state, and achieve fast transient response with periods of Transients 1 and 2. Similarly, when the load changes from 250 to 50 mA, as shown in Fig. 15(b), the fast transient mechanism also works precisely to improve the load transient response.

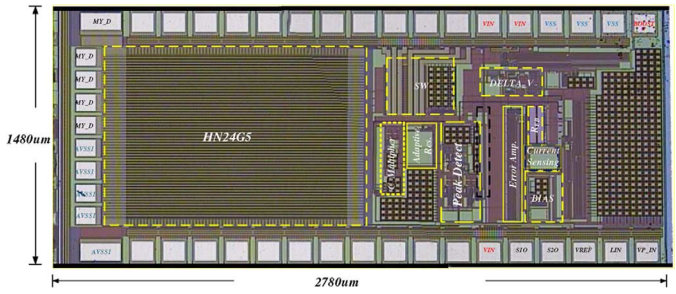

Fig. 17. Chip micrograph.

V. EXPERIMENTAL RESULTS

The proposed boost converter with the MHCC technique was fabricated by the TSMC 0.25 μm CMOS process. The off-chip inductor and output capacitor are 6.8 μH and 10 μF, respectively. The output voltage V_o is 12 V to drive three white LEDs in series. The specification is listed in Table III. The chip micrograph is shown in Fig. 17. The chip area is approximately 1480 μm $\times$ 2780 μm, including the test pads.

Experimental results of conventional boost converter are shown in Fig. 18. The input voltage is 4 V. The load current changes from 70 to 270 mA. The slew-rate load current is 100 mA/μs. The undershoot and overshoot voltages are 338 and 308 mV, respectively. The recovery time is 141 μs when the load current changes from light to heavy or from heavy to light. The load regulation is 0.16 mV/mA. The bandwidth is limited by the existence of the RHP zero. Under the low-bandwidth design, the transient response cannot be speeded up. Thus, the slow-response output voltage may cause the LEDs in series to have a little luminance variation when the dimming control is applied on the LED brightness control.

A comparison of the slow response of the conventional design and the experimental results of the proposed boost converter is shown in Fig. 19.

The undershoot and overshoot voltage are 300 and 234 mV, respectively. The recovery time of light to heavy load is 19.5 μs, and the recovery time of heavy to light load is 18.8 μs. Experimental results show that, compared with the conventional boost converter design, the improvement in the transient response is 7.2 times higher when the load current changes from light to heavy or vice versa. The improvement comes from the proposed HCC and the ACC techniques.

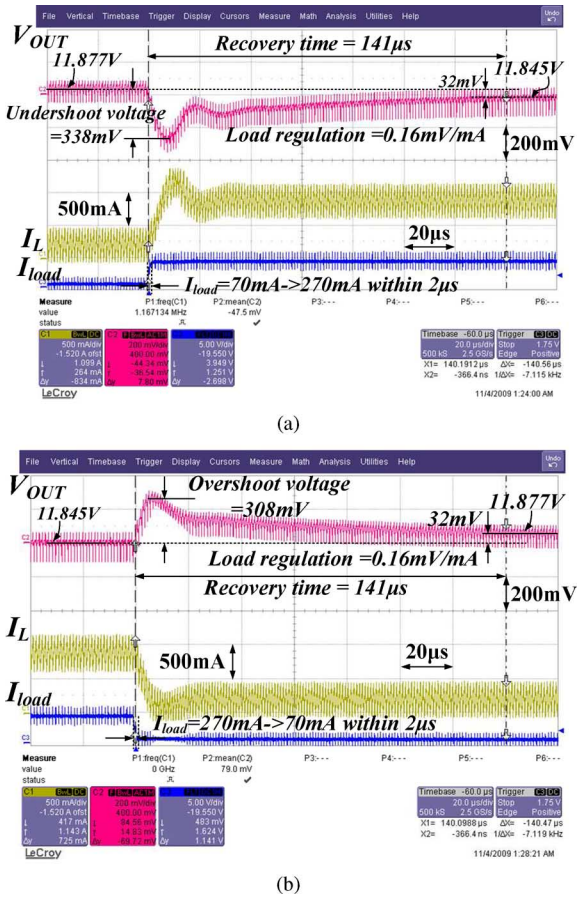

Fig. 18. Waveforms in conventional boost converter with HCC technique (a) when load current changes from 70 mA to 270 mA within 2 μs and (b) when load current changes from 270 to 70 mA within 2 μs.

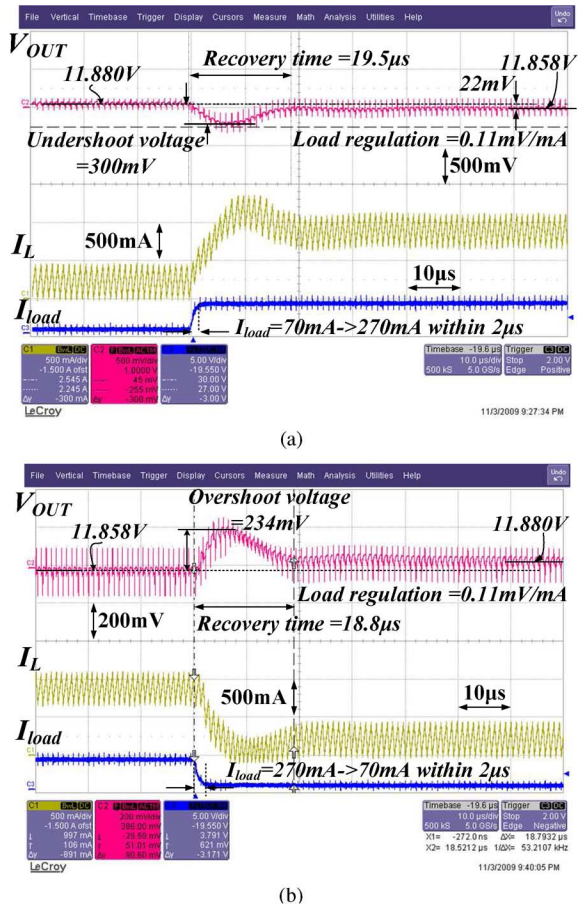

Fig. 19. Waveforms in the boost converter with the MHCC technique (a) when load current changes from 70 to 270 mA within 2 μs and (b) when load current changes from 270 to 70 mA within 2 μs.

The fast transient performance can be easily noted because the MHCC technique can speed up the transient response over a wide load current range, as shown in Fig. 20. The load current step decreases to approximately 100 and 50 mA, as shown in Figs. 20(a) and (b), respectively. The transient response time has only a slight improvement compared with that of the large load current step because the ACC technique has only a minimal effect on the whole system. Fortunately, the ACC technique consumes little power because it works only when the output voltage varies significantly. The power conversion efficiency is illustrated in Fig. 21. The power conversion efficiency is hardly influenced with or without the ACC technique. The power consumption overhead is merely 1%. The maximum power conversion efficiency is approximately 90%. A summary of the compared performances between the conventional and the proposed MHCC techniques is listed in Table IV.

VI. Conclusion

This paper proposes an MHCC technique to improve transient response of DC-DC boost converters. The ACC technique can settle the low-band value of the hysteresis generated by the error amplifier to further improve the transient response. Thus, the low bandwidth and large overshoot and undershoot voltages due to the RHP zero can be improved. The proposed

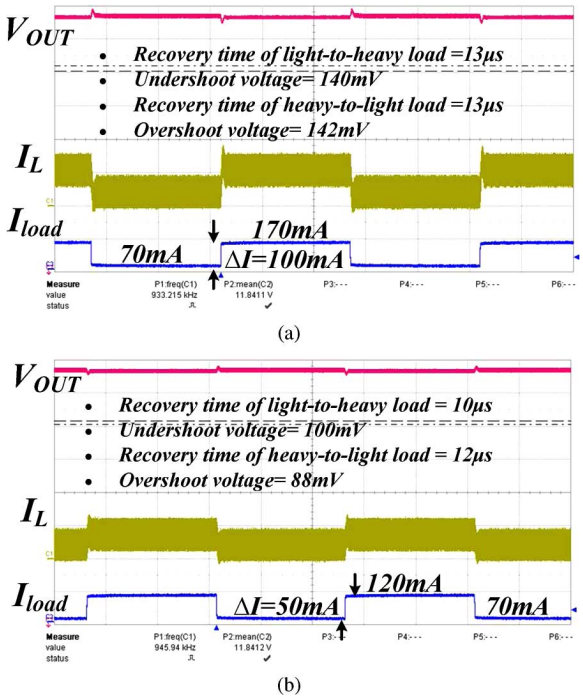

Fig. 20. Waveforms in the proposed boost converter with the MHCC technique when load current changes from light to heavy within 2 μs.

TABLE IV
COMPARISON OF THE CONVENTIONAL AND THE PROPOSED MHCC TECHNIQUES

Characteristics	Conditions	MHCC Technique	Conventional Technique
Supply Voltage	--	4V	4V
Output Voltage	--	12V	12V
Output Load Variation	--	200mA	200mA
Overshoot Voltage	I_{load}=270mA→70mA within 2μs	234mV	308mV
Undershoot Voltage	I_{load}=70mA→270mA within 2μs	300mV	338mV
Recovery time of heavy-to-light load	I_{load}=270mA→70mA @ 0.1% rated voltage within 2μs	18.8μs	141μs
Recovery time of light-to-heavy load	I_{load}=70mA→270mA @ 0.1% rated voltage within 2μs	19.5μs	141μs
Load Regulation	--	0.11mV/mA	0.16mV/mA

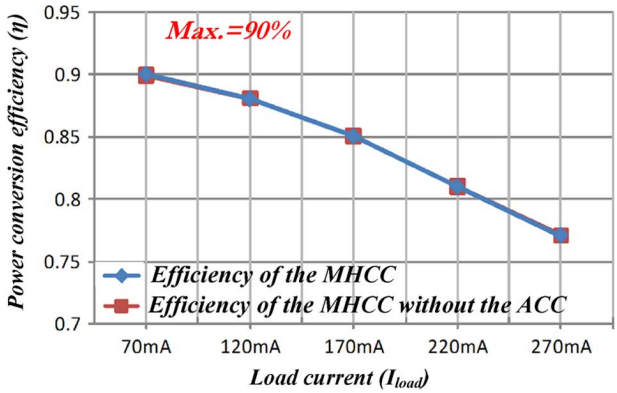

Fig. 21. Power conversion efficiency.

boost converter with the MHCC technique can demonstrate fast transient performance to verify its advantage in the driving capability of the LEDs in series. Good driving capability and accuracy can be guaranteed by the proposed MHCC technique according to the fast transient performance in the experimental results.

REFERENCES

[1] H.-J. Chiu and S.-J. Cheng, "LED backlight driving system for large-scale LCD panels," *IEEE Trans. Ind. Electron.*, vol. 54, no. 10, pp. 2751–2760, Oct. 2007.

[2] I.-H. Oh, "A single-stage power converter for a large screen LCD backlighting," in *Proc. Appl. Power Electron. Conf. Expo.*, Mar. 2006, pp. 1058–1063.

[3] C.-Y. Hsieh and K.-H. Chen, "Boost DC-DC converter with fast reference tracking (FRT) and charge-recycling (CR) techniques for high-efficiency and low-cost LED driver," *IEEE J. Solid-State Circuits*, vol. 44, no. 9, pp. 2568–2580, Sep. 2009.

[4] C.-H. Liu, Y.-C. Hsieh, T.-J. Tai, and K.-H. Chen, "SAR-controlled adaptive (SARCA) off-time control without sensing resistor for achieving high efficiency and Accuracy LED lighting system," *IEEE Trans. Circuits Syst. I, Reg. Papers*, vol. 57, no. 6, Jun. 2010.

[5] C.-Y. Hsieh, C.-Y. Yang, and K.-H. Chen, "A charge-recycling buck-store and boost-restore (BSBR) technique with dual outputs for RGB LED backlight and flashlight module," *IEEE Trans. Power Electron.*, vol. 24, no. 8, pp. 1914–1925, Aug. 2009.

[6] G. Jurasek, G. Levin, P. Sisson, and S. Repplinger, "High efficiency automotive power supply with hysteretic current mode controller," in *Proc. Appl. Power Electron. Conf. Expo.*, Mar. 1996, vol. 2, pp. 861–868.

[7] R. W. Erickson and D. Maksimovic, *Fundamentals of Power Electronics*, 2nd ed. Norwell, MA: Kluwer, 2001.

[8] C. Song and J. L. Nilles, "Accuracy analysis of hysteretic current-mode voltage regulator," in *Proc. Appl. Power Electron. Conf. Expo.*, Mar. 2005, vol. 1, pp. 276–280.

[9] W. Tang, F. C. Lee, and R. B. Ridley, "Small-signal modeling of average current-mode control," *IEEE Trans. Power Electron.*, vol. 8, no. 2, pp. 112–119, Apr. 1993.

[10] H.-W. Huang, K.-H. Chen, and S.-Y. Kuo, "Dithering skip modulation, width and dead time controllers in highly efficient DC-DC converters for system-on-chip applications," *IEEE J. Solid-State Circuits*, vol. 42, no. 11, pp. 2451–2465, Sep. 2009.

[11] H.-H. Huang, C.-L. Chen, and K.-H. Chen, "Adaptive window control (AWC) technique for hysteresis DC-DC buck converters with improved light and heavy load performance," *IEEE Trans. Power Electron.*, vol. 24, no. 6, pp. 1607–1617, Jun. 2009.

[12] B. Bryant and M. K. Kazimierczuk, "Small-signal duty cycle to inductor current transfer function for boost PWM DC-DC converter in continuous conduction mode," in *Proc. IEEE Int. Conf. Electron. Circuits Syst.*, May 2004, vol. 5, pp. 856–859.

[13] R. D. Middlebrook, "Modeling current-programmed buck and boost regulators," *IEEE Trans. Power Electron.*, vol. 4, no. 1, pp. 36–52, Jan. 1989.

[14] R. B. Ridley, "A new, continuous-time model for current-mode control," *IEEE Trans. Power Electron.*, vol. 6, no. 2, pp. 271–280, Apr. 1991.

[15] K.-H. Chen, C.-J. Chang, and T.-H. Liu, "Bidirectional current-mode capacitor multipliers for on-chip compensation," *IEEE Trans. Power Electron.*, vol. 23, no. 1, pp. 180–188, Jan. 2008.

[16] G. A. Rincón-Mora, "Active capacitor multiplier in Miller-compensated circuits," *IEEE J. Solid-State Circuits*, vol. 35, no. 1, pp. 26–32, Jan. 2000.

[17] B. Arbetter and D. Maksimović, "DC-DC converter with fast transient response and high efficiency for low-voltage microprocessor loads," in *Proc. Appl. Power Electron. Conf. Expo.*, Feb. 1998, vol. 1, pp. 156–162.

[18] F. Su, W.-H. Ki, and C.-Y. Tsui, "Ultra fast fixed-frequency hysteretic buck converter with maximum charging current control and adaptive delay compensation for DVS applications," *IEEE J. Solid-State Circuits*, vol. 43, no. 4, pp. 815–822, Apr. 2008.

[19] H. Guldemir, "Sliding mode control of DC-DC boost converter," *J. Appl. Sci.*, vol. 5, no. 3, pp. 588–592, 2005.

[20] D. Ge and Z. Chen, "On-chip boost DC-DC converter in color OLED driver & controller ICs for mobile application," in *Proc. IEEE ASICON*, Oct. 2005, vol. 1, pp. 459–463.

[21] T.-J. Tai and K.-H. Chen, "Switching loss calculation (SLC) and positive/negative compensated dynamic droop scaling (PNC-DDS) technique for high-efficiency multiple-input single-output (MISO) systems," *IEEE Trans. Power Electron.*, vol. 24, no. 5, pp. 1386–1398, May 2009.

[22] V. Gupta and G. A. Rincón-Mora, "Analysis and design of monolithic high PSR, linear regulators for SOC applications," in *Proc. IEEE SOC Conf.*, Sep. 2004, pp. 311–315.

[23] S. K. Hoon, S. Chen, F. Maloberti, J. Chen, and B. Aravind, "A low noise, high power supply rejection low dropout regulator for wireless system-on-chip applications," in *Proc. IEEE Custom Integr. Circuits Conf.*, Sep. 2005, pp. 759–762.

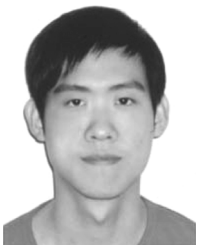

Jen-Chieh Tsai was born in Kaohsiung, Taiwan. He received the B.S. degree in the electrical engineering from National Yunlin University of Science and Technology, Yunlin, China, in 2003 and the M.S. degrees in the electrical engineering from Tamkang University, Taipei, in 2005, and is currently pursuing the Ph.D. degree in electrical and control engineering, National Chiao Tung University, Hsinchu, Taiwan.

His research area contains many projects of high resolution ADC, low power DAC and power management ICs at Low Power Mixed Signal Lab now. His interests include power management circuit designs, PFC ICs, and analog integrated circuit designs.

Chi-Lin Chen received the B.S. degree in Department of Electrical Engineering from Yuan Ze University, Taiwan, in 1995 and the M.S. degree in Department of Electrical Engineering from National Central University, Taiwan, in 1998. He is working toward the Ph.D. degree in the Department of Electrical and Control Engineering National Chiao Tung University, Hsinchu, Taiwan.

His interests include switching power circuit, mixed-signal circuit designs and analog integrated circuit designs.

Yu-Huei Lee (S'09) was born in Taipei, Taiwan. He received both B.S. and M.S. degrees from the Department of Electrical and Control Engineering, National Chiao Tung University, Hsinchu, Taiwan, in 2007 and 2009, respectively. He is currently pursuing the Ph.D. degree in the Institute of Electrical Control Engineering, National Chiao Tung University, Hsinchu, Taiwan.

He is a Faculty Member at the Mixed Signal and Power Management IC Laboratory, Institute of Electrical Control Engineering, National Chiao Tung University, Hsinchu, Taiwan. His current research interests include the power management integrated circuit design, light-emitting diode driver IC design, and analog integrated circuits.

Hong-Yuan Yang was born in Kaohsiung, Taiwan. He received the B.S. degree in electrical engineering from Feng Chia University, Taiwan, in 1992, and the M.S. degree in electrical and control engineering, National Chiao Tung University, Hsinchu, Taiwan in 2009.

He is currently an Analog Designer with Tontek Design Tech. Inc., Hsinchu, Taiwan. His interests include power management circuit designs, LED driver ICs, and low power analog integrated circuit designs.

Ming-Shen Hsu was born in Hsinchu, Taiwan. He received the B.S. degree in electrical engineering from Feng Chia University, Taiwan, in 1993, and the M.S. degree in electrical and control engineering, Chiao Tung University, Hsinchu, Taiwan in 2009.

He is now with Tontek Design Tech. Inc., Hsinchu, Taiwan, where He works on analog integrated-circuit design. His interests include analog and mixed-signal integrated circuit designs, power IC designs, and LED driver ICs.

Ke-Horng Chen (M'04-SM'09) received the B.S., M.S., and Ph.D. degrees in electrical engineering from National Taiwan University, Taipei, Taiwan, in 1994, 1996, and 2003, respectively.

From 1996 to 1998, he was a part-time IC Designer at Philips, Taipei. From 1998 to 2000, he was an Application Engineer at Avanti, Ltd., Taiwan. From 2000 to 2003, he was a Project Manager at ACARD, Ltd., where he was engaged in designing power management ICs. He is currently an Associate Professor in the Department of Electrical Engineering, National Chiao Tung University, Hsinchu, Taiwan, where he organized a Mixed-Signal and Power Management IC Laboratory. He is the author or coauthor of more than 80 papers published in journals and conferences, and also holds several patents. His current research interests include power management ICs, mixed-signal circuit designs, display algorithm and driver designs of liquid crystal display (LCD) TV, red, green, and blue (RGB) color sequential backlight designs for optically compensated bend (OCB) panels, and low-voltage circuit designs.